Environmental Science & Technology

pubs.acs.org/est

Article

Delineating the Relationship between Nanoparticle Attachment Efficiency and Fluid Flow Velocity

Changwoo Kim, Kurt D. Pennell, and John D. Fortner*

Cite This: *Environ. Sci. Technol.* 2020, 54, 13992−13999

Read Online

ACCESS | Metrics & More | Article Recommendations | Supporting Information

ABSTRACT: The ability to fundamentally describe nanoparticle (NP) transport in the subsurface underpins environmental risk assessment and successful material applications, including advanced remediation and sensing technologies. Despite considerable progress, our understanding of NP deposition behavior remains incomplete as there are conflicting reports regarding the effect of fluid flow velocity on attachment efficiency. To directly address this and more accurately describe NP attachment behavior, we have developed a novel protocol using a quartz crystal microbalance with dissipation monitoring (QCM-D) to separate and individually observe deposition mechanisms (diffusion and sedimentation), providing in situ, real-time information about particle diffusion (from the bulk liquid to solid surface). Through this technique, we have verified that the approaching velocity of NPs via diffusion increases (0.8−6.7 μm/s) with increasing flow velocity (6.1−106.0 μm/s), leading to an increased NP kinetic energy, thus affecting deposition processes. Further, in the presence of a secondary energy minimum associated with organic surface coatings, secondary minimum deposition decreases and primary minimum deposition increases with the flow velocity. NPs deposited at the primary minimum are relatively more resistant to hydrodynamic energies (including detachment associated energies), resulting in an increase of observed attachment efficiencies. Taken together, this work not only describes a novel method to delineate and quantify physical processes underpinning particle behavior but also provides direct measurements regarding key factors defining the relationship(s) of flow velocity and particle attachment. Such insight is valuable for next-generation fate and transport model accuracy, especially under unfavorable attachment regimes, which is a current and critical need for subsurface material applications and implication paradigms.

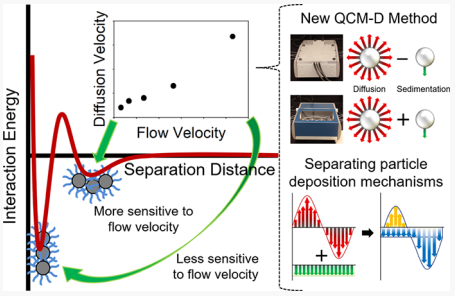

INTRODUCTION

Fundamentally observing and describing the behavior of both ubiquitous colloidal particles, including viruses, humic substances, clays, and engineered nanoparticles (NPs), is of broad research interest. With regard to subsurface fate and transport, NP deposition processes are critical for accurate modeling while being a challenge to directly measure.[1−4] Particle transport to the surface of solid media, which often referred to as the collector in colloid filtration theory (CFT), is governed by three distinct deposition (approaching) mechanisms: Brownian diffusion, interception, and sedimentation.[5,6] Once in contact with the collector surface, the stability of particle attachment can be described by the collective force and energy balances for the particle, collector surface, and fluid dynamics of the system.[6−8]

When approaching particle deposit under favorable conditions, meaning that the probability of the particle reaching a typically oppositely charged surface, making contact, and effectively staying attached is high (i.e., the absence of effective electrostatic double layer (EDL)),[8,9] transport and attachment trends can be predicted by colloid filtration theory (CFT). The CFT model was first developed by Yao et al.[5] for understanding traditional filtration unit operation. This derivation is based on the assumption that all particles in contact with the collector (termed as perfect sink) are removed from the suspension. Additionally, the collector (e.g., grains of sand, etc.) is considered to be an ideal, uniform shape (e.g., spherical) with a clean surface. To improve the initial CFT model, Rajagopalan and Tien adapted pore space geometry, termed as Happel's sphere-in-cell model.[10] Further, Tufenkji and Elimelech considered additional interactive energies, including thermal energy and interfacial van der Waals forces.[6] More recently, Long and Hilpert developed a correlation for diffusion-dominated particle transport by adapting lattice-Boltzmann simulations for randomly packed spheres.[11] Ma et al. explored CFT considering trajectory analysis, with a focus on particle rotation due to hydrodynamic retardation.[12,13] Nelson and Ginn have provided additional insight via a nonlinear regression of numerical data generated by Lagrangian simulations conducted with Happel's sphere-in-

Received: April 27, 2020
Revised: August 30, 2020
Accepted: September 30, 2020
Published: October 14, 2020

https://dx.doi.org/10.1021/acs.est.0c02669
Environ. Sci. Technol. 2020, 54, 13992−13999

cell porous media.[14] Ma et al. also developed a modified CFT model based on classic mass transfer relationships, which resulted in better prediction of collector efficiencies under low fluid velocity conditions.[15] While these models are well suited to describe favorable deposition conditions, predicting the behavior in unfavorable conditions (attachment efficiencies well below 1), which comprise a large fraction of environmental regimes, remains a challenge.[16]

In the presence of electrostatic repulsion forces between particles and collectors, attachment efficiency becomes the governing factor for determining particle deposition and transport.[1,17] Attachment efficiency is affected by both chemical (pH, ionic strength, and type) and physical factors (flow velocity, particle, and collector).[16] Regarding chemical aspects, there have been insightful studies focused on developing theoretical quantitative expressions based on Derjaguin−Landau−Verwey−Overbeek (DLVO) interactions.[1,18,19] While there is still room for quantitative improvement, governing theoretical expressions is qualitatively clear. For example, it is well known that high ionic strength suppresses the EDL of charged particles, resulting in increasing attachment efficiency.[1] In addition, divalent counterions significantly increase attachment efficiency through additional interactions, including bridging and cross-linking.[1,18]

Modeling the role of fluid flow parameters, and in particular flow velocity, as it relates to NP attachment efficiency, remains a challenge. Intuitively, attachment efficiency can be expected to be negligible (constant) or even decrease with increasing flow velocity as hydrodynamics can hinder attachment.[1,7,20,21] Computationally, Bai and Tien proposed a predictive framework for attachment efficiency in terms of flow velocity.[20,21] In their model, the hydrodynamic torque (from lift and drag forces) releases the deposited particles, resulting in decreasing attachment efficiency. Supporting this, several previous studies yielded results that were consistent with Bai and Tien's predictions of decreasing attachment efficiency with respect to the flow.[22−25] However, there have been a number of conflicting observations recently reported.[17,26−35] An empirical attachment efficiency model (correlating 80 data sets), developed by Phenrat et al., implies that the attachment efficiency increases as a function of the flow velocity,[27] contrary to the model of Bai and Tien.[20,21] For the Phenrat empirical model, only NPs that were surface-encapsulated with organic coatings were considered. Based on this work, the role of organic coating material(s) seems significant but is not specifically delineated. Without organic surface coatings (natural organic matter and/or artificial organic coating), increasing attachment efficiency trends have been also reported by others.[17,26,28,30,32,33,35]

Other system parameters, including surface heterogeneity, residual polymers/surfactants, and aggregation dynamics, have also been proposed as potentially sensitive variables when discerning unexpected attachment efficiency behavior(s).[1,2,29,36,37] In particular, physical heterogeneity, including nano- and microscale roughness, can influence particle retention and release.[38,39] For example, Rasmuson et al. verified that collector roughness increases the number of particle collisions under unfavorable conditions, observing a modest decrease in attachment.[40,9] Trauscht et al. also showed that nano- and microscale surface heterogeneities can enhance attachment.[41] Johnson et al. reported that, in certain cases, a poor prediction performance of CFT and attachment efficiencies can be attributed to wedging, in grain-to-grain contact geometries, and retention within secondary energy minima.[42] Wang et al. postulated that a free polymer (or free organic coating) competed with particles to attach the solid surface (especially near a column inlet), affecting particle attachmeant.[36] Further, organics adsorbed on collector surfaces may increase surface heterogeneities.[43] Additionally, the change of aggregate (bulk) density could lead to altered attachment efficiencies as decreased aggregate density results in poor estimations of collision number in terms of flow velocity.[1,2] To address such uncertainties, a reductionist approach evaluating ideal deposition systems with highly monodisperse particles, which can be monitored in situ and in real time, is needed.

The objective of this study is to elucidate the attachment efficiency relationship with respect to the flow velocity. For this, we have developed a microbalance-based methodology to delineate and quantify deposition processes. Properly employed, modern quartz crystal microbalance instrumentation is a powerful tool to elucidate deposition mechanisms as it allows for nanogram sensitivity under highly controlled conditions in addition to tunable surfaces (e.g., minimizing surface heterogeneities).[44] As model NPs, we chose two different sized (20 and 200 nm) monodisperse silica NPs with or without a surface coating ((3-aminopropyl)triethoxysilane, APTES). Detailed information regarding approaching particles, including velocity (via diffusion) along with the travel distance and time from the bulk (liquid phase) to the collector, is key for fundamentally describing attachment. By applying this new method, via operation of QCM-D in an inverted geometry, we directly calculated the particle velocity, distance, and time via diffusion (from the bulk (liquid phase) to the collector (solid phase)). Such empirical measurements have not been previously reported. Here, we quantitatively observe that the approaching diffusion velocity of NPs via diffusion increases as flow velocity is increased. For systems with significant secondary energy minima (as observed for NPs with organic surface coatings), a flow velocity increase can reduce secondary minimum deposition and enhance NPs' primary minimum deposition via increasing kinetic energy. We observe that such enhancement underpins an increasing attachment efficiency phenomenon previously observed in prior studies.[17,26−35]

MATERIALS AND METHODS

Silica Nanoparticles (NPs). Bare (hydroxylated) and coated ((3-aminopropyl)triethoxysilane ($C_9H_23NO_3Si$), APTES) 20 and 200 nm diameter silica NPs were purchased from nanoComposix. The average size and distribution of NPs were measured using transmission electron microscopy (TEM; Tecnai G2 Spirit, FEI) images with an Image Pro Plus 6.0 (Media Cybernetics, USA) by counting over 1000 NPs.[45] The hydrodynamic diameter (D_H) and zeta potential of the NPs were measured by dynamic light scattering (Malvern, Zetasizer Nano ZS, ZEN3600) in 1 mM NaCl at pH 7.2 and 22 °C. The number concentration of NPs was measured by considering the diameter of silica (measured by TEM) and silicon concentration, which was measured by inductively coupled plasma optical emission spectroscopy (ICP-OES; Perkin Elmer Optima 7300DV) with a 251.607 nm wavelength and radial view (detection limit: 0.9 μg/L). The organic coating loading mass per NP (also termed grafting density) was measured using a total organic carbon analyzer (TOC; Shimadzu Scientific Instrument).

https://dx.doi.org/10.1021/acs.est.0c02669
Environ. Sci. Technol. 2020, 54, 13992−13999

Quartz Crystal Microbalance with Dissipation (QCM-D). The deposition of NPs was monitored using QCM-D (Q-sense E4, Biolin Scientific) with a Q-sensor (5 MHz silica-coated QCM-D crystal, QSX-202, Q-sense). The flow velocity was controlled by a peristaltic pump (ISM935, ISMATEC, 0.0004−11 mL/min with 0.1% rpm resolution) and determined by considering the effective cross-sectional area of the measurement chamber (Q-chamber).

Measuring the Collector Efficiency. The deposition experiments were conducted in duplicate with four different NP concentrations in 1 mM NaCl at pH 7.2 and 22 °C under favorable conditions. Deposition of coated (positively charged) silica NPs was evaluated using negatively charged quartz Q-sensors (5 MHz AT-cut). For negatively charged, bare silica NPs, positively charged poly-L-lysine (PLL; Sigma Aldrich)-coated quartz sensors were used.[16] A QCM-D is a sensitive, frequency-based mass balance in the range of nanoscale (below 2 ng/cm^2).[46] Sauerbrey demonstrated a linear relationship between the deposited mass on the crystal (deposition on the sensor of QCM-D) and frequency shift; $\Delta m = C{\cdot}\Delta F_n/n$, whereby m is the deposited mass per unit area, C is the mass sensitivity constant (17.7 ng/cm^2 for a 5 MHz AT-cut quartz Q-sensor), F_n is the resonance frequency, and n is the resonance number (1, 3, 5, 7, 11, and 13).[47] By measuring the deposited mass per time, we can derive the collector efficiency by dividing the flux of NPs to the Q-chamber ($C_{NPs}{\cdot}Q$), where C_{NPs} is the mass concentration of NPs and Q is the flow rate (eq 1). We monitored all overtones (n) and selected the third n due to its stability.

$$\text{collector efficiency} = \frac{C{\cdot}\Delta F_n}{n{\cdot}\Delta t} \times \frac{1}{C_{NPs}{\cdot}Q} = \frac{\Delta m}{\Delta t} \times \frac{1}{C_{NPs}{\cdot}Q} = \frac{\text{deposited mass/time}}{\text{mass}_{in}/\text{time}} \quad (1)$$

As presented in Figures S1 and S2, each collector efficiency data point presented was obtained by linear regression of four different deposition signals (with experimental duplicates) as a function of NP concentration (total of eight sets of deposition tests). Corresponding regression statistics and analysis of variance (ANOVA) are presented in Table S1.

Measuring the Attachment Efficiency. The attachment efficiency (α) of NPs on quartz Q-sensors was evaluated by dividing the time-dependent frequency shift of the unfavorable condition to that of the favorable condition (eq 2).[48]

$$\alpha = \frac{(\Delta F_3/\Delta t)_{\text{unfavorable}}}{(\Delta F_3/\Delta t)_{\text{favorable}}} \quad (2)$$

Unfavorable deposition of coated (positively charged) silica NPs was evaluated using positively charged PLL-coated quartz Q-sensors. For bare silica NPs (negatively charged), negatively charged quartz Q-sensors were used. All tests were conducted in duplicate with four different NP concentrations in varying ionic concentrations (0.2 M NaCl for 20 nm NPs, 0.1 M for 200 nm bare NPs, and 0.25 M NaCl for 200 nm coated NPs in pH 7.2) to get a clear frequency signal. All deposition experiments measuring attachment efficiency used the same Q-sensor (including coatings). As presented in Figures S3 and S4, each attachment efficiency data point was obtained by linear regression of four different deposition signals (with experimental duplicates) as a function of NP concentration (total of eight sets of deposition tests). For each, regression statistics and ANOVA are presented in Table S2.

Protocol for Poly-L-lysine (PLL) Coating. Positively charged Q-sensors were evaluated by coating a Q-sensor with PLL. First, we rinsed the quartz sensors in 10 mM HEPES buffer (4-(2-hydroxyethyl)-1-piperazineethanesulfonic acid) and 100 mM NaCl for 10 min. Then, we coated the quartz sensors using 0.1 g/L PLL in 10 mM HEPES buffer and 100 mM NaCl solution. After the signal stabilized, we rinsed the quartz sensor again for 10 min using 10 mM HEPES buffer in 100 mM NaCl solution (Figure S5).[16] The PLL coating thickness was calculated based on a viscoelastic model within QTools software (Q-Sense AB, Vastra Frolunda, Sweden), as described by others.[49]

Velocity via Diffusion (V_d) and Sedimentation (V_g). NP V_d was calculated using the following relationship[50,51]

$$\frac{\int_0^{2\pi} V_d \sin\theta + V_g d\theta}{\int_0^{2\pi} V_d \sin\theta - V_g d\theta} = \frac{\text{collector efficiency(inverted mode)}}{\text{collector efficiency(normal mode)}} \quad (3)$$

Based on calculated V_d, time over a distance (x, thickness of diffusion boundary layer) can be obtained by eqs 4 and 5, as derived from the Stokes−Einstein relationship[50]

$$D = \frac{k_B T}{3\pi\mu d} \quad (4)$$

where D is the bulk diffusion coefficient, k_B is the Boltzmann constant, and T is the absolute temperature.

$$V_d = \frac{x}{t} = \frac{2D}{x} \quad (5)$$

The settling velocity (V_g) can be obtained by Stoke's equation (eq 6)[51]

$$V_g = \frac{g(\rho_p - \rho_w)d^2}{18\mu} \quad (6)$$

Here, g is the acceleration caused by gravity, ρ_p is the density of NP, ρ_w is the density of water, d is the diameter of the NP, and μ is the viscosity of the solution.

Derjaguin, Landau, Verwey, and Overbeek (DLVO) Interaction Energies. The classical DLVO theory was used to calculate the interaction energies between silica and the Q-sensor for all deposition experimental conditions.[2] Details are described in the Supporting Information.

Torque Applied to Deposited NP. Torque energy applied to deposited NP was calculated using experimental velocity conditions.[43,52] Details are described in the Supporting Information.

RESULTS AND DISCUSSION

Effect of Flow Velocity on Attachment Efficiency. Flow velocity is considered to be an important factor for evaluating the attachment efficiency as deposited NPs can be resuspended, via flow dynamics, under the unfavorable conditions.[53] Before exploring the flow velocity effects under the unfavorable conditions, we investigated favorable deposition with varied flow velocities. Two different sized (20 and 200 nm) silica NPs, with or without a surface coating

https://dx.doi.org/10.1021/acs.est.0c02669
Environ. Sci. Technol. 2020, 54, 13992−13999

(APTES), were evaluated in five different flow velocity conditions (6.1, 13.2, 26.5, 52.9, and 106.0 μm/s), which cover a range of typical subsurface environmental relevant flow velocities (5.2−31.3 μm/s).[54] Ionic strength and pH were held constant for all experiments, at 1 mM NaCl and pH 7.2, respectively. A schematic diagram of bare and coated NPs is presented in Figure S6. The point of zero charge (PZC) of bare silica NPs is 1.5−3.7 (negatively charged above this pH) due to hydroxyl functionality.[55] The surface of the coated silica NPs is the covered amine group (positively charged). Zeta potentials of 20 and 200 nm bare NPs and 20 and 200 nm coated NPs were −9.3 and −41.0 mV and 9.1 and 39.6 mV, respectively. Detailed information for characterization of NPs, including the TEM image, size histograms, hydrodynamic diameter (number mean and volume mean), NP mass, mass of coating (grafting density), and zeta potential, can be found in the Supporting Information (Figure S7 and Tables S3 and S4). Also, favorable depositions conditions were also theoretically confirmed from DLVO energy profiles, which show no energy barrier (Figure S8).

As shown in Figure 1a, the collector efficiency determined under favorable conditions for 20 nm NPs (regardless of coating) decreases with increasing flow velocity as the total number of collisions decreases with the increased flow velocity.[2,6] The collector efficiencies were 0.32, 0.28, 0.20, 0.18, and 0.14 for 20 nm bare NPs in 6.1, 13.2, 26.5, 52.9, and 106.0 μm/s flow rates, respectively. For coated 20 nm NPs, the collector efficiencies were 0.28, 0.23, 0.19, 0.16, and 0.12 in 6.1, 13.2, 26.5, 52.9, and 106.0 μm/s flow rates, respectively. Figure 1b presents a collector efficiency of 200 nm NPs as a function of flow velocity. The collector efficiencies obtained under favorable conditions for bare NPs were 0.187, 0.133, 0.078, 0.044, and 0.028 with increasing flow velocity, and the collector efficiencies of coated NPs were 0.180, 0.104, 0.062, 0.035, and 0.020 with increasing flow velocity. Similar to 20 nm NPs, the collector efficiencies of both bare and coated 200 nm NPs decreased with increasing flow velocity due to the decrease of collisions with the surface via diffusion.[2,6] The NP collector efficiency slope (200 nm), as a function of flow velocity, is higher than 20 nm NPs, indicating that larger particles are more sensitive to change in flow conditions. This is similar to what is observed in a CFT model as a function of the Peclet number.[6]

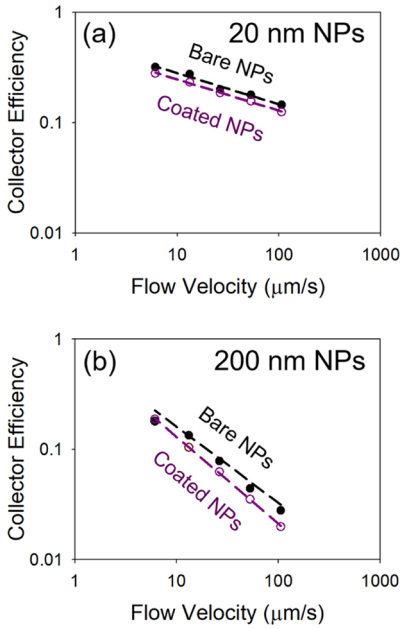

Figure 1. Collector efficiency of (a) 20 and (b) 200 nm NPs as a function of flow velocity. The black dashed linear regression line is for bare NPs, and the purple dashed linear regression line is for coated NPs. The collector efficiency was evaluated in 1 mM NaCl at pH 7.2 (under favorable deposition conditions).

We next explored the deposition of NPs as a function of flow velocity under unfavorable conditions. For this comparison, particle attachment must produce a mass change resulting from a deposition of NPs that is large enough to provide a clearly detectable frequency signal with the QCM-D. Through an initial screening, we found that the varying salinity for each NP provided a sufficient frequency signal without NP aggregation. Though the zeta potential of NPs decreases in the presence of increasing ionic strength, NPs remained highly monodisperse, with no size difference compared to low ionic strength conditions (Figure S9). Observed particle stability can be attributed to the charged hydroxyl and amine groups on the surface of silica. Zeta potentials of 20 and 200 nm bare NPs and 20 and 200 nm coated NPs were −7.0 and −10.1 mV and 6.8 and 14.8 mV, respectively. For unfavorable conditions, DLVO energies of each deposition scenario are calculated and presented in Figure S10. The highest primary maximum values were observed at 8.3 and 201.6 k_BT and 1.4 and 508.7 k_BT for 20 and 200 nm bare NPs and 20 and 200 nm coated NPs, respectively. For deposition of coated NPs under unfavorable conditions, steric repulsion, effectively in the range of the molecular size (length) at the surface, should also be considered.[56] Here, we calculated the PLL coating (on the surface Q-sensor) to be ca. 4.5 nm (Figure S11), which is similar to other reports.[57]

As presented in Figure 2, attachment efficiency of bare NPs decreased for 20 nm while remaining near constant for 200 nm with increasing flow velocity. These results match well with previous attachment efficiency model equations developed by Elimelech[1] and Bai and Tien.[20,21] While the torque applied to 200 nm NPs is higher than 20 nm particles (Figure S12), the attachment efficiency of bare 200 nm NPs is less sensitive to flow velocity. This is due to the fact that the primary energy barrier (needed to overcome for detachment) is size-dependent,[58] as presented in Figure S10. The attachment efficiency of surface-coated NPs increases with increasing flow velocity for the range of flow velocities evaluated (up to 26.5 μm/s for 20 nm NPs and 13.2 μm/s for 200 nm NPs) and then decreases, though the torque-applied NPs increases with increasing the flow velocity (Figure S12). Several studies have reported increasing attachment efficiency with respect to the flow velocities for NPs coated with organic coatings.[27,29] Collector roughness (porous media)[59] and aggregation[1,2] were proposed as possible reasons. In this study, excess collector roughness and aggregation of NPs are negligible as we use clean, smooth collector surfaces[60,61] and highly monodisperse NPs, which do not aggregate over experimental time frames and stated conditions.

Here, we hypothesize that unexpected attachment efficiency observations (i.e., increasing with velocity) result from the presence of secondary energy minima. According to the classical Derjaguin−Landau−Verwey−Overbeek (DLVO) theory, the secondary minimum can play a significant role in deposition of large colloids (e.g., 1000 nm).[2,62] However, with

https://dx.doi.org/10.1021/acs.est.0c02669
Environ. Sci. Technol. 2020, 54, 13992−13999

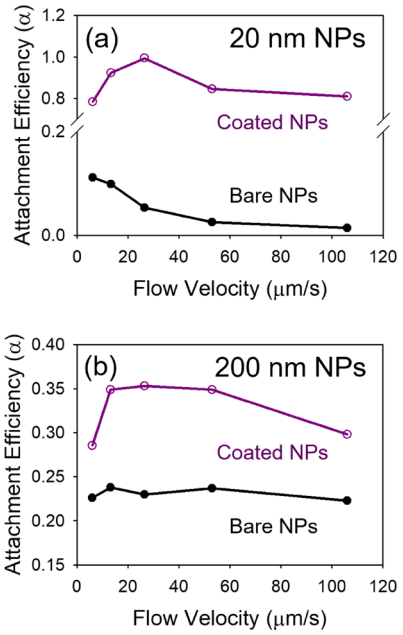

Figure 2. (a) Attachment efficiency of 20 nm bare (black) and coated (purple) NPs as a function of the flow velocity under relatively unfavorable conditions. (b) Attachment efficiency of 200 nm bare (black) and coated (purple) NPs as a function of flow velocity. The attachment efficiency was measured in 0.2 M NaCl for 20 nm NPs, 0.1 M for 200 nm bare NPs, and 0.25 M NaCl for 200 nm coated NPs at pH 7.2 (under unfavorable deposition conditions).

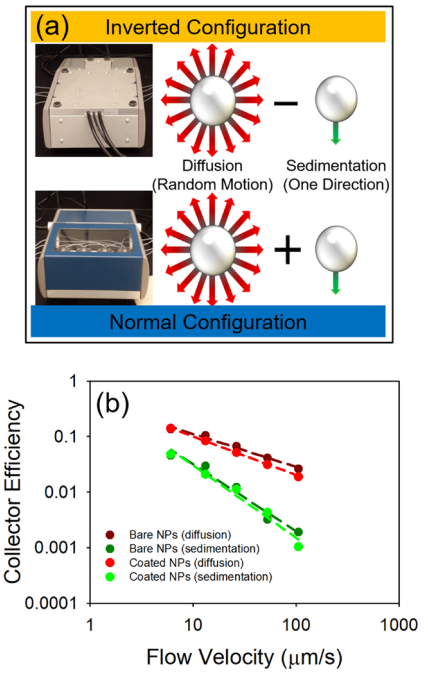

Figure 3. (a) Depiction of NP transport via diffusion and sedimentation in normal and inverted QCM-D configurations. (b) Collector efficiency resulting from diffusion and sedimentation for 200 nm bare and coated NPs as a function of flow velocity. Every test was conducted in 1 mM NaCl at pH 7.2 (under favorable deposition conditions).

organic coating, elastic−steric and osmotic repulsion interaction energies can be significant under high ionic strength as EDL repulsion decreases.[63] To better understand this, we have quantified several particle deposition parameters, including the velocity, distance, and time of NPs via diffusion, as discussed below.

Exploring the Attachment Efficiency and Flow Velocity Relationship. To separate individual deposition mechanisms (i.e., diffusion, sedimentation, and interception), the QCM-D was operated in both normal and inverted configurations at five flow velocities (6.1, 13.2, 26.5, 52.9, and 106.0 μm/s) in 1 mM NaCl at pH 7.2. The QCM-D sensor (module) geometry provides an undisturbed flow field, which is essential for theoretical analysis. For undisturbed flow, inertia (interception) plays no role in deposition (Levich−Smoluchowski approximation);[2] thus, diffusion and sedimentation can be isolated. To separate the individual mechanisms, we focus on 200 nm NPs as the sedimentation velocity is readily measurable.

The possible velocity vectors of diffusion (via Brownian motion) and sedimentation (via gravity) for NPs are presented in Figure 3a. When the QCM-D is operated in a normal configuration, gravity acts in the deposition direction, and when inverted, it acts opposite to the direction of deposition. The driving forces for NPs deposition in the normal QCM-D configuration are thus diffusion and sedimentation (diffusion + sedimentation), but gravity hinders the deposition of NPs in the inverted QCM-D configuration (diffusion − sedimentation). The separated collector efficiencies of 200 nm bare and coated NPs are presented in Figure 3b, whereby diffusion is the governing mechanism for all conditions explored. Here, for the first time, the NP velocity, distance, and time traveled (from bulk (liquid phase) to the collector (solid phase)) were directly quantified as they relate to individual deposition mechanisms (e.g., diffusion and sedimentation). This is contrast to other approaches such as from Cho et al.[64] who calculated the NP velocity, via diffusion (V_d), by assuming a constant travel distance (e.g., 1 mm). As diffusion acts equally in all directions via Brownian random motion, and sedimentation proceeds in only one direction, as it is driven by gravity (Figure 3a), the two can be separated here. As shown in Figure 4a, the sum of the Y axes of every velocity vector via diffusion is $V_d \cdot \sin\theta$ (0−360°), and the settling velocity (V_g) acts only downward (−90°). Hence, the total of the velocity vectors (Y axis) of NPs in the normal QCM-D configuration is $V_d \cdot \sin\theta + V_g$. For an inverted mode, it is $V_d \cdot \sin\theta - V_g$. The velocity, via diffusion (V_d), can be calculated as the ratio of the collector efficiency for a normal configuration to inverted configuration, which is proportional to the ratio of the positive area (yellow) to the negative area (blue) of $V_d \cdot \sin\theta + V_g$ from 0 to 360° (Figure 4a). As presented in Figure 4b, the V_d of both bare and coated NPs increased with increasing flow velocity. Conversely, the thickness of the diffusion boundary layer and time, for both NPs, decreases with increasing flow velocity (Figure 4c and Figure S13). As particle kinetic energy is directly related to velocity ($(0.5 \cdot m_{NP} \cdot V)$ here, m_{NP} is the mass of the NP and V is the velocity of the NP), higher kinetic energies are thus reached at higher flow rates due to the hydrodynamic stream. A higher kinetic energy will increase the ratio of NPs deposited on the primary minimum instead of the secondary minimum, and thus, the probability of detachment by hydrodynamic forces becomes lower,[52,65] resulting in an increasing attachment efficiency with increasing flow velocity.

Interestingly, we also observed that sedimentation significantly affects attachment efficiency (under unfavorable

https://dx.doi.org/10.1021/acs.est.0c02669
Environ. Sci. Technol. 2020, 54, 13992−13999

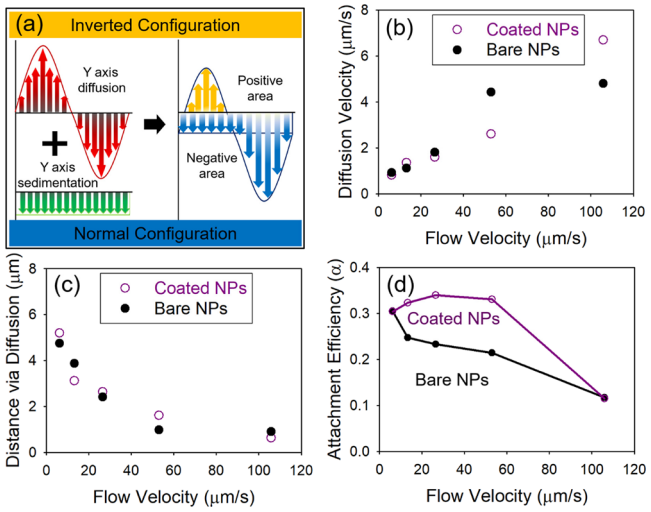

Figure 4. (a) Depiction of vector sums for *Y* axes of motion from diffusion and sedimentation. (b) Velocity via diffusion and (c) distance for 200 nm bare (black) and coated (purple) NPs traveled (from bulk (liquid phase) to the collector (solid phase)) as a function of flow velocity. (d) Attachment efficiency of 200 nm bare (black) and coated (purple) NPs as a function of flow velocity under inverted QCM-D operation. The attachment efficiency was measured in 0.1 M NaCl for 200 nm bare NPs and 0.25 M NaCl for 200 nm coated NPs at pH 7.2 (unfavorable deposition conditions).

conditions) under higher flow velocity conditions, even though diffusion is the dominant transport mechanism for these systems. Comparing Figures 2b and 4d, the attachment efficiencies of the normal and inverted configurations were similar, except for the highest flow velocity conditions. The attachment efficiency in normal mode was considerably higher than in the inverted mode at the highest flow velocity evaluated (106.0 μm/s). This flow velocity is the maximum flow velocity recommended by the QCM-D manufacturer to avoid unwanted pressure fluctuations and/or any hydrodynamic turbulence. We also experimentally verified system stability at these flow rates for all configurations (>20 h).[66] Recognizing that, as the integrated force balance(s) become(s) more complex under unfavorable conditions and increasing the applied torque (via relatively higher flow velocities), it appears that gravity can have a (potential) role in deposition stability for these systems. Based on such observations, the diameter and density of NPs, in addition to flow conditions and geometries, are critical when considering subsurface transport processes under unfavorable conditions. Further, when considering applications with higher flow fields, such as biomedical applications, diameter and density of NPs will also be critical to consider as the blood flow velocity is much higher (3.0×10^{-4} to 4.0×10^{-1} m/s)[67,68] than typical groundwater velocities.

To conclude, using a newly developed QCM protocol, we measured the V_d of NPs by vector deconvolution in situ and in real time to directly observe NP V_d increasing with flow velocity. In the presence of secondary minima, NP deposition on the primary minimum leads to increased attachment with increased flow velocity due to increased kinetic energies. These data highlight that, to describe or predict the transport of nanoscale particles, the attachment efficiency and flow velocity relationship need to be carefully considered when a significant secondary minimum is present, for example, when the hydrodynamic diameter is large (e.g., above 1 μm) and/or coated with organic substance(s). Looking forward, using these and similar techniques, NP attachment behavior under unfavorable conditions for heterogeneous surfaces and upper collector geometries at high(er) flow velocities should be further considered.

■ ASSOCIATED CONTENT

Supporting Information

The Supporting Information is available free of charge at https://pubs.acs.org/doi/10.1021/acs.est.0c02669.

QCM-D experiment data set, Q-sensor coating protocol, characterizations of silica NPs, thickness of the PLL coating, DLVO energy interactions, the time-dependent diameters of silica NPs, the calculated applied torque energy, and time via diffusion for silica NPs (PDF)

■ AUTHOR INFORMATION

Corresponding Author

John D. Fortner − *Department of Chemical and Environmental Engineering, Yale University, New Haven, Connecticut 06520, United States;* orcid.org/0000-0002-3669-779X; Phone: +1-314-935-9293; Email: john.fortner@yale.edu

Authors

Changwoo Kim − *Department of Chemical and Environmental Engineering, Yale University, New Haven, Connecticut 06520, United States;* orcid.org/0000-0002-8117-842X

Kurt D. Pennell − *Civil and Environmental Engineering, Brown University, Providence, Rhode Island 02912, United States;* orcid.org/0000-0002-5788-6397

Complete contact information is available at: https://pubs.acs.org/10.1021/acs.est.0c02669

Notes

The authors declare no competing financial interest.

■ ACKNOWLEDGMENTS

This work is supported by the U.S. Army Corps of Engineers (W912HZ-13-2-0009-P00001), the U.S. Department of Agriculture, NIFA (2018-67021-28319), and the U.S. National Science Foundation (CBET 1437820 and CBET 1704326). TEM, DLS, ICP-OES, and TOC were provided by the Nano Research Facility (NRF) at Washington University in St. Louis. The authors acknowledge Professor James C. Ballard for reviewing the manuscript.

■ REFERENCES

(1) Elimelech, M. Predicting collision efficiencies of colloidal particles in porous media. *Water Res.* **1992**, *26*, 1−8.

(2) Elimelech, M.; Gregory, J.; Jia, X. *Particle deposition and aggregation: measurement, modelling and simulation*; Butterworth-Heinemann: 2013.

(3) Ju-Nam, Y.; Lead, J. R. Manufactured nanoparticles: an overview of their chemistry, interactions and potential environmental implications. *Sci. Total Environ.* **2008**, *400*, 396−414.

(4) Wiesner, M. R.; Lowry, G. V.; Alvarez, P.; Dionysiou, D.; Biswas, P. *Assessing the risks of manufactured nanomaterials*; ACS Publications: 2006.

(5) Yao, K.-M.; Habibian, M. T.; O'Melia, C. R. Water and waste water filtration. Concepts and applications. *Environ. Sci. Technol.* **1971**, *5*, 1105−1112.

(6) Tufenkji, N.; Elimelech, M. Correlation equation for predicting single-collector efficiency in physicochemical filtration in saturated porous media. *Environ. Sci. Technol.* **2004**, *38*, 529−536.
(7) Johnson, W. P.; Tong, M. Observed and simulated fluid drag effects on colloid deposition in the presence of an energy barrier in an impinging jet system. *Environ. Sci. Technol.* **2006**, *40*, 5015−5021.
(8) VanNess, K.; Rasmuson, A.; Ron, C. A.; Johnson, W. P. A Unified Force and Torque Balance for Colloid Transport: Predicting Attachment and Mobilization under Favorable and Unfavorable Conditions. *Langmuir* **2019**, *35*, 9061−9070.
(9) Rasmuson, A.; VanNess, K.; Ron, C. A.; Johnson, W. P. Hydrodynamic versus surface interaction impacts of roughness in closing the gap between favorable and unfavorable colloid transport conditions. *Environ. Sci. Technol.* **2019**, *53*, 2450−2459.
(10) Rajagopalan, R.; Tien, C. Trajectory analysis of deep-bed filtration with the sphere-in-cell porous media model. *AIChE J.* **1976**, *22*, 523−533.
(11) Long, W.; Hilpert, M. A correlation for the collector efficiency of Brownian particles in clean-bed filtration in sphere packings by a Lattice-Boltzmann method. *Environ. Sci. Technol.* **2009**, *43*, 4419−4424.
(12) Ma, H.; Pedel, J.; Fife, P.; Johnson, W. P. Hemispheres-in-cell geometry to predict colloid deposition in porous media. *Environ. Sci. Technol.* **2009**, *43*, 8573−8579.
(13) Ma, H.; Johnson, W. P. Colloid retention in porous media of various porosities: Predictions by the hemispheres-in-cell model. *Langmuir* **2010**, *26*, 1680−1687.
(14) Nelson, K. E.; Ginn, T. R. New collector efficiency equation for colloid filtration in both natural and engineered flow conditions. *Water Resour. Res.* **2011**, *47*, W05543.
(15) Ma, H.; Hradisky, M.; Johnson, W. P. Extending applicability of correlation equations to predict colloidal retention in porous media at low fluid velocity. *Environ. Sci. Technol.* **2013**, *47*, 2272−2278.
(16) Seetha, N.; Raoof, A.; Kumar, M. S. M.; Hassanizadeh, S. M. Upscaling of nanoparticle transport in porous media under unfavorable conditions: Pore scale to Darcy scale. *J. Contam. Hydrol.* **2017**, *200*, 1−14.
(17) Toloni, I.; Lehmann, F.; Ackerer, P. Modeling the effects of water velocity on TiO_2 nanoparticles transport in saturated porous media. *J. Contam. Hydrol.* **2014**, *171*, 42−48.
(18) Shen, C.; Huang, Y.; Li, B.; Jin, Y. Predicting attachment efficiency of colloid deposition under unfavorable attachment conditions. *Water Resour. Res.* **2010**, *46*, W11526.
(19) Shen, C.; Li, B.; Huang, Y.; Jin, Y. Kinetics of coupled primary- and secondary-minimum deposition of colloids under unfavorable chemical conditions. *Environ. Sci. Technol.* **2007**, *41*, 6976−6982.
(20) Bai, R.; Tien, C. A new correlation for the initial filter coefficient under unfavorable surface interactions. *J. Colloid Interface Sci.* **1996**, *179*, 631−634.
(21) Bai, R.; Tien, C. Particle deposition under unfavorable surface interactions. *J. Colloid Interface Sci.* **1999**, *218*, 488−499.
(22) Du, Y.; Shen, C.; Zhang, H.; Huang, Y. Effects of flow velocity and nonionic surfactant on colloid straining in saturated porous media under unfavorable conditions. *Transp. Porous media* **2013**, *98*, 193−208.
(23) Rahman, T.; Millwater, H.; Shipley, H. J. Modeling and sensitivity analysis on the transport of aluminum oxide nanoparticles in saturated sand: Effects of ionic strength, flow rate, and nanoparticle concentration. *Sci. Total Environ.* **2014**, *499*, 402−412.
(24) Zhang, Z.; Gao, P.; Qiu, Y.; Liu, G.; Feng, Y.; Wiesner, M. Transport of cerium oxide nanoparticles in saturated silica media: influences of operational parameters and aqueous chemical conditions. *Sci. Rep.* **2016**, *6*, 34135.
(25) Sasidharan, S.; Bradford, S. A.; Torkzaban, S.; Ye, X.; Vanderzalm, J.; Du, X.; Page, D. Unraveling the complexities of the velocity dependency of *E. coli* retention and release parameters in saturated porous media. *Sci. Total Environ.* **2017**, *603-604*, 406−415.
(26) Lecoanet, H. F.; Wiesner, M. R. Velocity effects on fullerene and oxide nanoparticle deposition in porous media. *Environ. Sci. Technol.* **2004**, *38*, 4377−4382.
(27) Phenrat, T.; Song, J. E.; Cisneros, C. M.; Schoenfelder, D. P.; Tilton, R. D.; Lowry, G. V. Estimating attachment of nano- and submicrometer-particles coated with organic macromolecules in porous media: development of an empirical model. *Environ. Sci. Technol.* **2010**, *44*, 4531−4538.
(28) Kocur, C. M.; O'Carroll, D. M.; Sleep, B. E. Impact of nZVI stability on mobility in porous media. *J. Contam. Hydrol.* **2013**, *145*, 17−25.
(29) Kim, C.; Lee, S. Effect of seepage velocity on the attachment efficiency of TiO_2 nanoparticles in porous media. *J. Hazard. Mater.* **2014**, *279*, 163−168.
(30) Kokkinos, P.; Syngouna, V. I.; Tselepi, M. A.; Bellou, M.; Chrysikopoulos, C. V.; Vantarakis, A. Transport of human adenoviruses in water saturated laboratory columns. *Food Environ. Virol.* **2015**, *7*, 122−131.
(31) Prédélus, D.; Lassabatere, L.; Louis, C.; Gehan, H.; Brichart, T.; Winiarski, T.; Angulo-Jaramillo, R. Nanoparticle transport in water-unsaturated porous media: effects of solution ionic strength and flow rate. *J. Nanopart. Res.* **2017**, *19*, 104.
(32) Syngouna, V. I.; Chrysikopoulos, C. V.; Kokkinos, P.; Tselepi, M. A.; Vantarakis, A. Cotransport of human adenoviruses with clay colloids and TiO_2 nanoparticles in saturated porous media: Effect of flow velocity. *Sci. Total Environ.* **2017**, *598*, 160−167.
(33) Zhang, C.; Yan, A.; Wang, G.; Jin, C.; Chen, Y.; Shen, C. Impact of flow velocity on transport of graphene oxide nanoparticles in saturated porous media. *Vadose Zone J.* **2018**, *17*, 180019.
(34) Lim, M.; Hwang, G.; Bae, S.; Jang, M.-H.; Choi, S.; Kim, H.; Hwang, Y. S. Transport of citrate-coated silver nanoparticles in saturated porous media. *Environ. Geochem. Health* **2020**, 1753−1766.
(35) Zhao, W.; Zhao, P.; Tian, Y.; Shen, C.; Li, Z.; Jin, C. Transport and retention of Microcystis aeruginosa in porous media: Impacts of ionic strength, flow rate, media size and pre-oxidization. *Water Res.* **2019**, *162*, 277−287.
(36) Wang, Y.; Becker, M. D.; Colvin, V. L.; Abriola, L. M.; Pennell, K. D. Influence of residual polymer on nanoparticle deposition in porous media. *Environ. Sci. Technol.* **2014**, *48*, 10664−10671.
(37) Li, Y.; Wang, Y.; Pennell, K. D.; Abriola, L. M. Investigation of the transport and deposition of fullerene (C60) nanoparticles in quartz sands under varying flow conditions. *Environ. Sci. Technol.* **2008**, *42*, 7174−7180.
(38) Bradford, S. A.; Torkzaban, S. Determining Parameters and Mechanisms of Colloid Retention and Release in Porous Media. *Langmuir* **2015**, *31*, 12096−12105.
(39) Shen, C.; Jin, Y.; Zhuang, J.; Li, T.; Xing, B. Role and importance of surface heterogeneities in transport of particles in saturated porous media. *Crit. Rev. Environ. Sci. Technol.* **2020**, *50*, 244−329.
(40) Rasmuson, A.; Pazmino, E.; Assemi, S.; Johnson, W. P. Contribution of nano- to microscale roughness to heterogeneity: Closing the gap between unfavorable and favorable colloid attachment conditions. *Environ. Sci. Technol.* **2017**, *51*, 2151−2160.
(41) Trauscht, J.; Pazmino, E.; Johnson, W. P. Prediction of nanoparticle and colloid attachment on unfavorable mineral surfaces using representative discrete heterogeneity. *Langmuir* **2015**, *31*, 9366−9378.
(42) Johnson, W. P.; Tong, M.; Li, X. On colloid retention in saturated porous media in the presence of energy barriers: The failure of α, and opportunities to predict η. *Water Resour. Res.* **2007**, *43*, DOI: 10.1029/2006WR005770.
(43) Ryan, J. N.; Elimelech, M. Colloid mobilization and transport in groundwater. *Colloids Surf., A* **1996**, *107*, 1−56.
(44) Dixon, M. C. Quartz crystal microbalance with dissipation monitoring: enabling real-time characterization of biological materials and their interactions. *J. Biomol. Tech.* **2008**, *19*, 151.

(45) Vigneau, E.; Loisel, C.; Devaux, M. F.; Cantoni, P. Number of particles for the determination of size distribution from microscopic images. *Powder Technol.* **2000**, *107*, 243−250.
(46) Carton, I.; Brisson, A. R.; Richter, R. P. Label-free detection of clustering of membrane-bound proteins. *Anal. Chem.* **2010**, *82*, 9275−9281.
(47) Sauerbrey, G. Verwendung von Schwingquarzen zur Wägung dünner Schichten und zur Mikrowägung. *Z. Phys.* **1959**, *155*, 206−222.
(48) Chen, K. L.; Elimelech, M. Interaction of fullerene (C60) nanoparticles with humic acid and alginate coated silica surfaces: measurements, mechanisms, and environmental implications. *Environ. Sci. Technol.* **2008**, *42*, 7607−7614.
(49) Parveen, N.; Jana, P. K.; Schönhoff, M. Viscoelastic properties of polyelectrolyte multilayers swollen with ionic liquid solutions. *Polymer* **2019**, *11*, 1285.
(50) Hiemenz, P. C.; Rajagopalan, R. *Principles of Colloid and Surface Chemistry, revised and expanded*; CRC press: 2016, DOI: 10.1201/9781315274287.
(51) Teeguarden, J. G.; Hinderliter, P. M.; Orr, G.; Thrall, B. D.; Pounds, J. G. Particokinetics in vitro: dosimetry considerations for in vitro nanoparticle toxicity assessments. *Toxicol. Sci.* **2007**, *95*, 300−312.
(52) Li, X.; Zhang, P.; Lin, C. L.; Johnson, W. P. Role of hydrodynamic drag on microsphere deposition and re-entrainment in porous media under unfavorable conditions. *Environ. Sci. Technol.* **2005**, *39*, 4012−4020.
(53) Franchi, A.; O'Melia, C. R. Effects of natural organic matter and solution chemistry on the deposition and reentrainment of colloids in porous media. *Environ. Sci. Technol.* **2003**, *37*, 1122−1129.
(54) Johnson, R. L.; Pankow, J. F. Dissolution of dense chlorinated solvents into groundwater. 2. Source functions for pools of solvent. *Environ. Sci. Technol.* **1992**, *26*, 896−901.
(55) Shchukin, E. D.; Pertsov, A. V.; Amelina, E. A.; Zelenev, A. S. *Colloid and surface chemistry*; Elsevier: 2001.
(56) Hotze, E. M.; Phenrat, T.; Lowry, G. V. Nanoparticle aggregation: challenges to understanding transport and reactivity in the environment. *J. Environ. Qual.* **2010**, *39*, 1909−1924.
(57) Etienne, O.; Picart, C.; Taddei, C.; Haikel, Y.; Dimarcq, J. L.; Schaaf, P.; Voegel, J. C.; Ogier, J. A.; Egles, C. Multilayer polyelectrolyte films functionalized by insertion of defensin: a new approach to protection of implants from bacterial colonization. *Antimicrob. Agents Chemother.* **2004**, *48*, 3662−3669.
(58) Polte, J. Fundamental growth principles of colloidal metal nanoparticles−a new perspective. *CrystEngComm* **2015**, *17*, 6809−6830.
(59) Das, S. K.; Schechter, R. S.; Sharma, M. M. The role of surface roughness and contact deformation on the hydrodynamic detachment of particles from surfaces. *J. Colloid Interface Sci.* **1994**, *164*, 63−77.
(60) Choi, J.-H.; Kim, S.-O.; Linardy, E.; Dreaden, E. C.; Zhdanov, V. P.; Hammond, P. T.; Cho, N.-J. Influence of pH and surface chemistry on poly (L-lysine) Adsorption onto solid supports investigated by quartz crystal microbalance with dissipation monitoring. *J. Phys. Chem. B* **2015**, *119*, 10554−10565.
(61) Macakova, L.; Blomberg, E.; Claesson, P. M. Effect of adsorbed layer surface roughness on the QCM-D response: focus on trapped water. *Langmuir* **2007**, *23*, 12436−12444.
(62) Litton, G. M.; Olson, T. M. Particle size effects on colloid deposition kinetics: Evidence of secondary minimum deposition. *Colloids Surf., A* **1996**, *107*, 273−283.
(63) Mosley, L. M.; Hunter, K. A.; Ducker, W. A. Forces between colloid particles in natural waters. *Environ. Sci. Technol.* **2003**, *37*, 3303−3308.
(64) Cho, E. C.; Zhang, Q.; Xia, Y. The effect of sedimentation and diffusion on cellular uptake of gold nanoparticles. *Nat. Nanotechnol.* **2011**, *6*, 385−391.
(65) Torkzaban, S.; Bradford, S. A.; Walker, S. L. Resolving the coupled effects of hydrodynamics and DLVO forces on colloid attachment in porous media. *Langmuir* **2007**, *23*, 9652−9660.
(66) Mafi, R.; Pelton, R. H. Emulsion/surface interactions from quiescent quartz crystal microbalance measurements with an inverted sensor. *Langmuir* **2015**, *31*, 7238−7241.
(67) Marieb, E. N.; Hoehn, K. *The Cardiovascular system: blood vessels. Human anatomy & physiology*. Pearson Education, Inc.: Upper Saddle River, NJ, 2013.
(68) Tortora, G. J.; Derrickson, B. The cardiovascular system: blood vessels and hemodynamics. In *Principals of anatomy and physiology*; 7th edn. Harper Collins College: 2012, 610−632.

https://dx.doi.org/10.1021/acs.est.0c02669
Environ. Sci. Technol. 2020, 54, 13992−13999